Turkish Journal of Physics

http://journals.tubitak.gov.tr/physics/

Research Article

Turk J Phys
(2020) 44: 39 – 48

doi:10.3906/fiz-1906-8

The effect of temperature on fusion cross-sections of the ^{8}B proton halo nucleus

Murat AYGÜN*
Department of Physics, Faculty of Arts and Sciences, Bitlis Eren University, Bitlis, Turkey

Received: 13.06.2019 • **Accepted/Published Online:** 07.01.2020 • **Final Version:** 12.02.2020

Abstract: In the present study, I investigate the effect of temperature on fusion cross-sections of the ^{8}B proton halo projectile. For this purpose, I evaluate two different fusion reactions, ^{8}B + ^{28}Si and ^{8}B +^{58}Ni, in the available literature. I apply two different nuclear potentials as a function of temperature. I calculate both fusion cross-sections and nuclear potentials for both reactions and I then compare the theoretical results with the experimental data. This comparison provides an opportunity for a test of different temperature-dependent potentials in explaining the fusion cross-sections with the ^{8}B halo nucleus.

Key words: Temperature dependence, fusion reactions, halo nuclei

1. Introduction

Fusion reaction is one of the most interesting topics of nuclear physics. Fusion reactions are generally considered as complete and incomplete fusion reactions. In this context, the calculations of fusion cross-sections are generally carried out at zero temperature. However, if a collision between two nuclei occurs, it leads to an increase in temperature [1]. Thus, they can be in an excited state [2]. This may cause a change in both fusion cross-section and interaction potential. Therefore, I consider that temperature-dependent analysis of cross-sections of fusion reactions would be beneficial to better understand fusion interactions.

^{8}B is one of the most interesting proton halo nuclei. It is short-lived, and it has very small proton separation energy, such as 0.138 MeV [3]. Fusion studies on the ^{8}B proton halo nucleus are scarce owing to both a limited number of laboratories and experimental challenges [4,5], although many studies have addresses scattering reactions. The first fusion experiment regarding ^{8}B was performed for the ^{8}B +^{58}Ni reaction at near-Coulomb barrier energies by Aguilera et al. [6]. Amador-Valenzuela et al. [3] examined possible model dependency in the involved $\sigma_p \rightarrow \sigma_{fus}$ mapping of the ^{8}B + ^{58}Ni reaction. Camacho et al. [7] carried out a simultaneous analysis for elastic scattering and fusion cross-sections of ^{8}B +^{58}Ni reaction. Later, the experimental data of the ^{8}B +^{28}Si fusion reaction were reported for four different near-barrier energies by Pakou et al. [4]. However, the temperature-dependent changes of these reactions have not been previously investigated. Therefore, I suggest that it would be useful to know temperature-dependent changes in describing ^{8}B fusion cross-sections.

The aim of this study is to examine the temperature dependence of both fusion cross-sections and interaction potentials of ^{8}B +^{28}Si and ^{8}B +^{58}Ni reactions. With this goal, the nuclear potentials are calculated for two different versions, which consist of the temperature-dependent potential used in the fusion calculations

*Correspondence: maygun@beu.edu.tr

by Tomasi [8] and the temperature-dependent proximity potential [9–13]. The fusion cross-sections for these reactions are then obtained at different temperatures values from 0 to 5 MeV. Finally, theoretical results and experimental data are compared with each other.

Section 2 provides a brief summary of the theoretical analysis. Section 3 presents the results and discussion. Section 4 gives the conclusions.

2. Theoretical process

The total effective potential for fusion cross-section calculations can be written as the sum of Coulomb and nuclear potentials in the following form:

$$V_{\text{Total}}(r) = V_{\text{Coulomb}}(r) + V_{\text{Nuclear}}(r), \tag{1}$$

where the Coulomb potential [14] due to a charge $Z_P e$ interacting with a charge $Z_T e$ distributed uniformly over a sphere of radius R_c is:

$$V_{\text{Coulomb}}(r) = \frac{1}{4\pi\varepsilon_0}\frac{Z_P Z_T e^2}{r} \qquad r \geq R_C \tag{2}$$

$$= \frac{1}{4\pi\varepsilon_0}\frac{Z_P Z_T e^2}{2R_C}\left(3\text{-}\frac{r^2}{R_C^2}\right), \qquad r < R_C\,, \tag{3}$$

$$R_C = 1.25(A_P^{\frac{1}{3}} + A_T^{\frac{1}{3}}). \tag{4}$$

The nuclear potential is the sum of real and imaginary potentials. The real potential is obtained by using two different potentials depending on temperature, which are described in the following subsections. However, the imaginary potential is taken as Woods–Saxon (WS) potential given by

$$W(r) = -i\frac{W_0}{1+\exp(\frac{r-R_w}{a_w})}, R_w = r_w(A_P^{\frac{1}{3}} + A_T^{\frac{1}{3}}), \tag{5}$$

where A_P and A_T are the masses of projectile and target nuclei, W_0 is the depth value, r_w is the radius parameter, and a_w is the diffuseness parameter. In theoretical analysis of both ^{8}B $+^{28}$Si and ^{8}B $+^{58}$Ni fusion reactions, I have researched the potential parameters (W_0, r_w, and a_w) at intervals of 0.1 and 0.01 fm in order to achieve good agreement with the experimental data. While determining the parameters, I have tried to keep them as constant as possible at different temperature values of the same reaction. I have carried out this process for ^{8}B $+^{28}$Si and ^{8}B $+^{58}$Ni reactions separately. The values of the potential parameters are listed in Table 1 for the ^{8}B $+^{28}$Si reaction and in Table 2 for the ^{8}B $+^{58}$Ni reaction. The FRESCO code [15,16] has been used for the fusion cross-section calculations. For this purpose, proximity and Tomasi potentials have been first obtained for each reaction and temperature by using a FORTRAN code written by me. The resulting values were then run with the FRESCO program. Thus, the fusion cross-sections for each potential and reaction at different temperatures have been achieved.

Table 1. Potential parameters for ^{8}B $+^{28}$Si fusion cross-section calculated by using the proximity and Tomasi potentials for the real part and the Woods–Saxon potential for the imaginary part.

Potential	Parameter	T = 0	T = 1	T = 2	T = 3	T = 4	T = 5
Proximity	W_0 (MeV)	3.1	3.0	2.8	2.7	2.6	2.41
	r_w(fm)	1.2	1.2	1.2	1.2	1.2	1.2
	a_w(fm)	0.8	0.8	0.8	0.8	0.8	0.8
Tomasi	W_0 (MeV)	3.1	2.75	2.5	1.8	1.5	1.4
	r_w(fm)	0.9	0.8	0.8	0.8	0.8	0.8
	a_w(fm)	0.4	0.7	0.7	0.7	0.7	0.7

Table 2. Same as Table 1, but for ^{8}B $+^{58}$Ni reaction.

Potential	Parameter	T = 0	T = 1	T = 2	T = 3	T = 4	T = 5
Proximity	W_0 (MeV)	16.9	16.9	16.9	16.9	15.9	15.4
	r_w(fm)	1.4	1.4	1.4	1.4	1.4	1.4
	a_w(fm)	0.8	0.8	0.8	0.8	0.8	0.8
Tomasi	W_0 (MeV)	16.6	8.0	7.9	3.0	2.1	2.0
	r_w(fm)	1.4	1.0	1.0	1.0	1.0	1.0
	a_w(fm)	0.8	0.4	0.4	0.4	0.4	0.4

2.1. Nuclear potential type I

The first potential examined as temperature-dependent in this study is Tomasi potential. Tomasi et al. [8] carried out calculations for both different systems and different temperatures. They obtained an $\overline{r}$ value for each temperature. Finally, they parametrized nuclear potential type I as in [17,18]. This potential is given by [8]:

$$V_N(S) = \frac{A_1^{\frac{1}{3}} A_2^{\frac{1}{3}}}{A_1^{\frac{1}{3}} + A_2^{\frac{1}{3}}} U_N(S,T), \tag{6}$$

where

$$U_N(S,T) = \begin{cases} a(T)\ \exp(-b(T)S^2), & \text{for } S \geq 0, \\ a(T)\ + cS^2, & \text{for } S < 0, \end{cases} \tag{7}$$

$$S(T) = R - \overline{r}(T)(A_1^{\frac{1}{3}} + A_2^{\frac{1}{3}}), \tag{8}$$

$$\overline{r}(T) = 0.86 - 0.0119T^2, \tag{9}$$

$$a(T) = -36 - 2.55T^2, \tag{10}$$

$$b(T) = 0.2135 - 0.05088T + 0.003821T^2, \tag{11}$$

$$c = 4.82. \tag{12}$$

2.2. Nuclear potential type II

The second potential depending on temperature is Proximity 1977 (Prox 77). The proximity model proposed by Blocki et al. [19] is one of the most important models used to determine fusion reactions. In the proximity model, the proximity potential is written based on both a geometric factor and a universal function. In this respect, various versions of the proximity potential, which can change by radius parameter, surface energy coefficient, and universal function, can be obtained from the literature. Proximity 1977, Proximity 1979, Proximity 1981, Proximity 1984, Proximity 1988, Proximity 1995, Proximity 2003, and Proximity 2010 are some of them. It is also known that proximity potentials are based on Proximity 1977 potential. As a result of this, different studies have been conducted to determine the validity of proximity potentials in explaining the fusion cross-sections [20–24]. For example, the best proximity potential for the empirical barrier distribution model (EBDM) has been found as Proximity 1977. Additionally, Proximity 1977 potential has been established as a temperature-dependent effect. Therefore, I have used Proximity 1977 potential for temperature-dependent calculations in this study. It is parameterized by [19]:

$$V_N(r) = 4\pi\gamma b\overline{R}\Phi\left(\zeta = \frac{r - C_1 - C_2}{b}\right) \text{ MeV}, \tag{13}$$

where

$$\overline{R} = \frac{C_1 C_2}{C_1 + C_2}, \qquad C_i = R_i\left[1 - \left(\frac{b}{R_i}\right)^2 + ...\right]. \tag{14}$$

R_i, the effective radius, is

$$R_i = 1.28A_i^{1/3} - 0.76 + 0.8A_i^{-1/3} \text{ fm} \qquad (i = 1, 2). \tag{15}$$

γ, the surface energy coefficient, is

$$\gamma = \gamma_0\left[1 - k_s\left(\frac{N - Z}{N + Z}\right)^2\right], \tag{16}$$

where $N(Z)$ is the total number of neutrons (protons), γ_0 is 0.9517 MeV/fm^2, and k_s is 1.7826 [25]. The universal function, $\Phi(\zeta)$, is given by

$$\Phi(\zeta) = \begin{cases} -\frac{1}{2}(\zeta - 2.54)^2 - 0.0852(\zeta - 2.54)^3, & \text{for } \zeta \leq 1.2511, \\ -3.437\exp\left(-\frac{\zeta}{0.75}\right), & \text{for } \zeta \geq 1.2511. \end{cases} \tag{17}$$

Temperature dependence values are assumed as [9–13]:

$$b(T) = b(T = 0)[1 + 0.009T^2], \tag{18}$$

$$R_i(T) = R_i(T = 0)[1 + 0.0005T^2] \quad \text{fm} \qquad (i = 1, 2). \tag{19}$$

3. Results and discussion

3.1. Analysis of ^{8}B + ^{28}Si fusion reaction

I have examined the fusion cross-section of the ^{8}B + ^{28}Si reaction in the available literature. In Table 1, the potential parameters of ^{8}B + ^{28}Si fusion cross-sections calculated by using proximity and Tomasi potentials for

the real part and Woods–Saxon potential for the imaginary part are listed. The real parts of nuclear potentials obtained with the help of proximity and Tomasi potentials are compared in Figure 1. In this sense, Figure 1a demonstrates the results of proximity potential and Figure 1b displays the results of Tomasi potential. It is observed that the real potentials decrease while the temperature values increase from 0 to 5 MeV. Also, they extend at larger distances, and their locations are shifted at smaller distances.

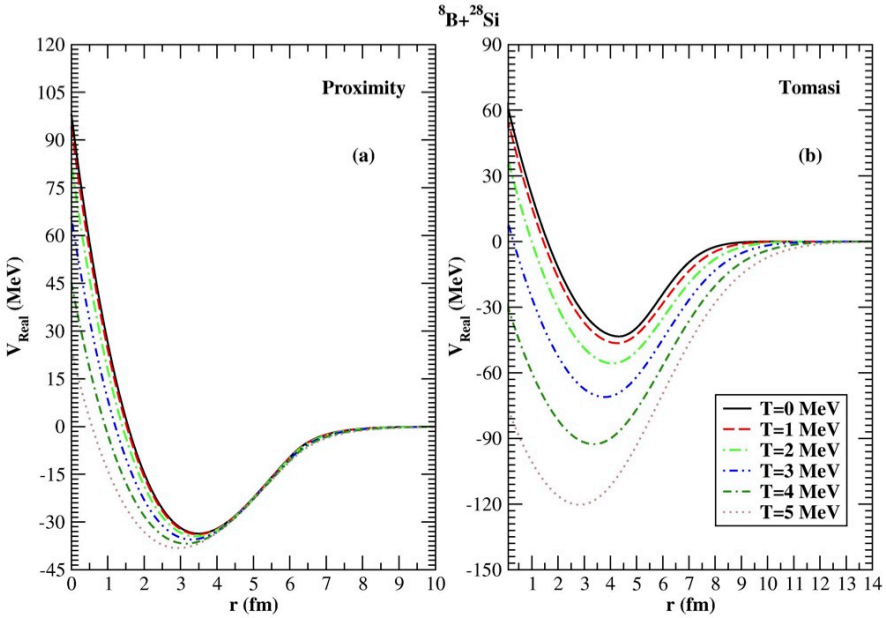

Figure 1. Comparison of the real potentials of the ^{8}B + ^{28}Si interaction potential for different values of the temperature.

I give a comparison of the cross-sections of the ^{8}B + ^{28}Si fusion reaction calculated for proximity and Tomasi potentials as both temperature-dependent and temperature-independent in Figure 2. Also, the fusion cross-sections that are obtained for different temperatures from 0 to 5 MeV are compared with the experimental data. I observe that the results of proximity potential (Figure 2a) are more evident after 3 MeV while the results of Tomasi potential (Figure 2b) show differences for each temperature value. The results of proximity potential are more smooth, whereas an oscillating structure in the results of Tomasi potential is observed. While proximity results are very close to each other between 0 and 3 MeV, the results for 4 and 5 MeV are slightly different. Also, the results of proximity potential are in good agreement with the experimental data. On the other hand, it is realized that the results of Tomasi potential at T = 0 and 1 MeV are in slightly better agreement with the data in comparison with other temperature values.

3.2. Analysis of ^{8}B+ ^{58}Ni fusion reaction

Other fusion experimental data measured related to the ^{8}B proton halo nucleus are for the ^{8}B +^{58}Ni system. Thus, in this part, we focus on the cross-section of the ^{8}B +^{58}Ni fusion reaction. With this goal, we investigate the fusion cross-section and the real part of nuclear potential. Figure 3 exhibits a comparison of the real parts of two different nuclear potentials, namely proximity (Figure 3a) and Tomasi (Figure 3b) potentials. Table 2 gives the imaginary potential parameters used in the cross-section calculations of the ^{8}B +^{58}Ni fusion reaction. It is seen that the real parts of the potentials decrease with increasing temperature values from 0 to 5 MeV. This

state is similar to the results of ^{8}B $+^{28}$Si reaction. Also, they extend at larger distances and their locations are shifted at smaller distances.

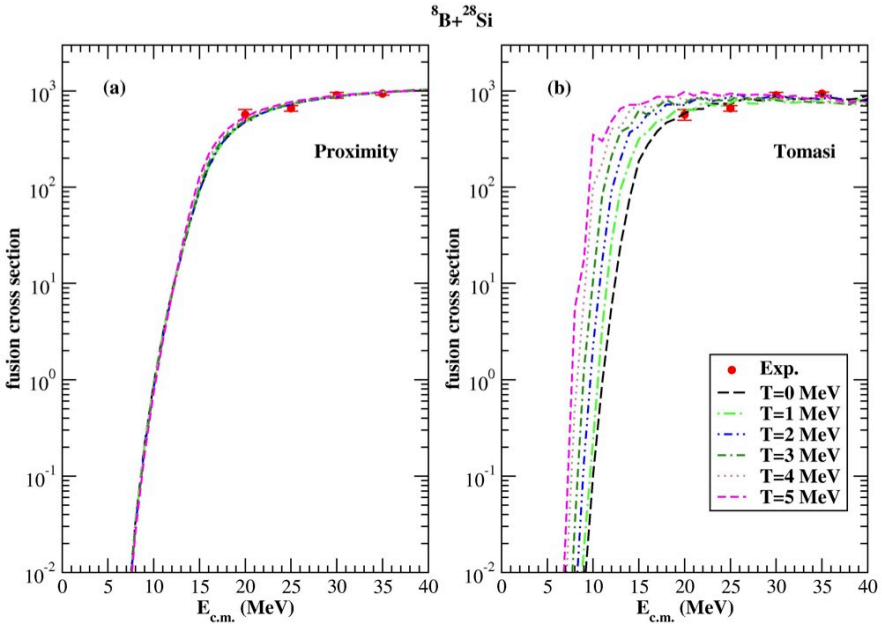

Figure 2. Comparison of the experimental data and the theoretical results of ^{8}B $+^{28}$Si fusion reaction calculated for two different potentials. The experimental data are taken from [4].

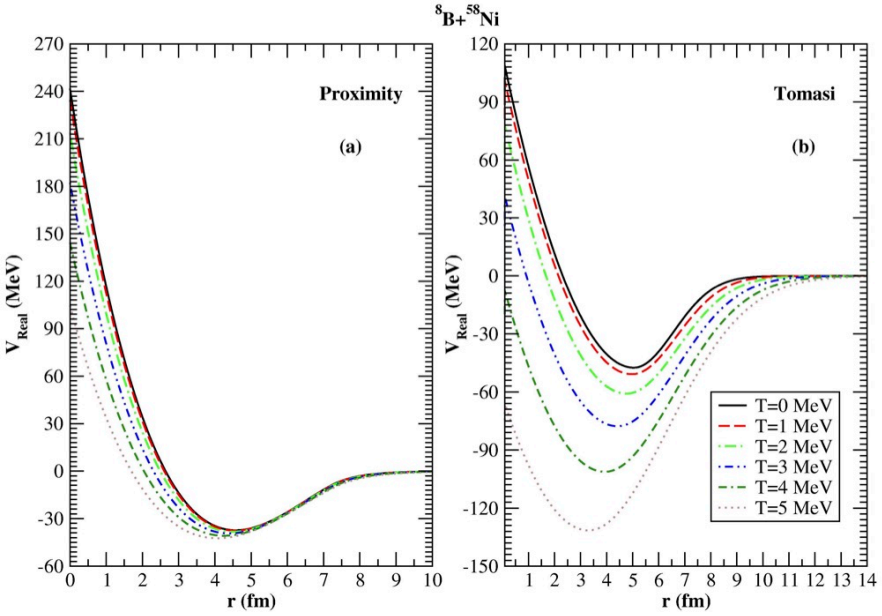

Figure 3. Comparison of the real potentials of the ^{8}B + ^{58}Ni interaction potential for different values of the temperature.

Figure 4 displays the cross-sections of the ^{8}B $+^{58}$Ni fusion reaction for proximity and Tomasi potentials as temperature-dependent (T = 1, 2, 3, 4, and 5 MeV) and temperature-independent (T = 0 MeV). It is observed

that the results of proximity potential (Figure 4a) are very similar to each other for different temperatures, while the results of Tomasi potential (Figure 4b) show differences at each temperature value. Hence, the fusion cross-sections of the ^{8}B $+^{58}$Ni reaction for different temperature values are the same for the proximity potential and the results are in agreement with the experimental data. On the other hand, it can be seen from Figure 4b that the results of Tomasi potential at T = 0 are generally consistent with the data, but they are inadequate in the explanation of some experimental data at low energies. However, it has been observed that the results of Tomasi potential have changed with increasing temperature. It has also been noticed that the agreement between the results for Tomasi potential and experimental data clearly increases at T = 3 MeV. Additionally, it can be said that the result of Tomasi potential at T = 3 MeV is better than the other temperature results of Tomasi potential. I can deduce that the fusion cross-sections with Tomasi potential are more sensitive to temperature than proximity potential.

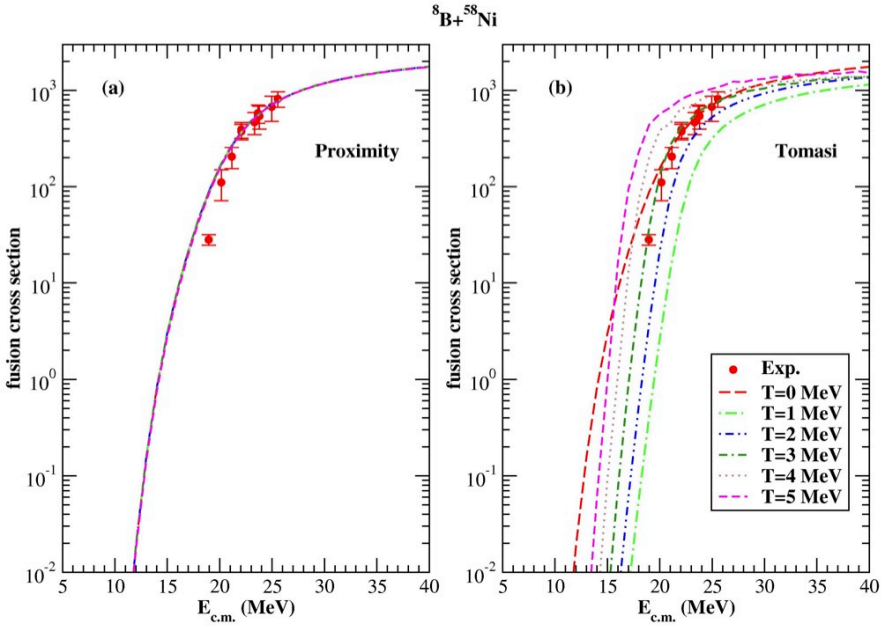

Figure 4. Comparison of the experimental data and the theoretical results of ^{8}B $+^{58}$Ni fusion reaction calculated for two different potentials. The experimental data are taken from [6].

When I examine the W_0 values of both proximity and Tomasi potentials of the ^{8}B $+^{28}$Si reaction from Table 1, I observe that the W_0 values of both potentials vary depending on the temperature. In this context, it can be seen that the W_0 values decrease with increasing temperature. When I evaluate the W_0 values of proximity and Tomasi potentials given for the ^{8}B $+^{58}$Ni reaction in Table 2, I notice that the W_0 values decrease with the increase of the temperature, similar to the ^{8}B $+^{28}$Si reaction. Similar behaviors observed in both reactions can be considered as a parameter indicating the suitability of the theoretical calculations.

Figure 5 shows the variations with r of the imaginary potentials obtained for both proximity (Figure 5a) and Tomasi (Figure 5b) potentials of the ^{8}B $+^{28}$Si reaction according to the values in Table 1. Figure 6 similarly presents the variations with r of the imaginary potentials obtained for proximity (Figure 6a) and Tomasi (Figure 6b) potentials of the ^{8}B $+^{58}$Ni reaction according to the values in Table 2. It can be seen from Figures 5 and 6 that the W_0 values of the imaginary part of the ^{8}B $+^{58}$Ni system are highly sensitive to the

temperature variations, especially in Tomasi potential. This may be due to either the structure of the target nucleus or the experimental data.

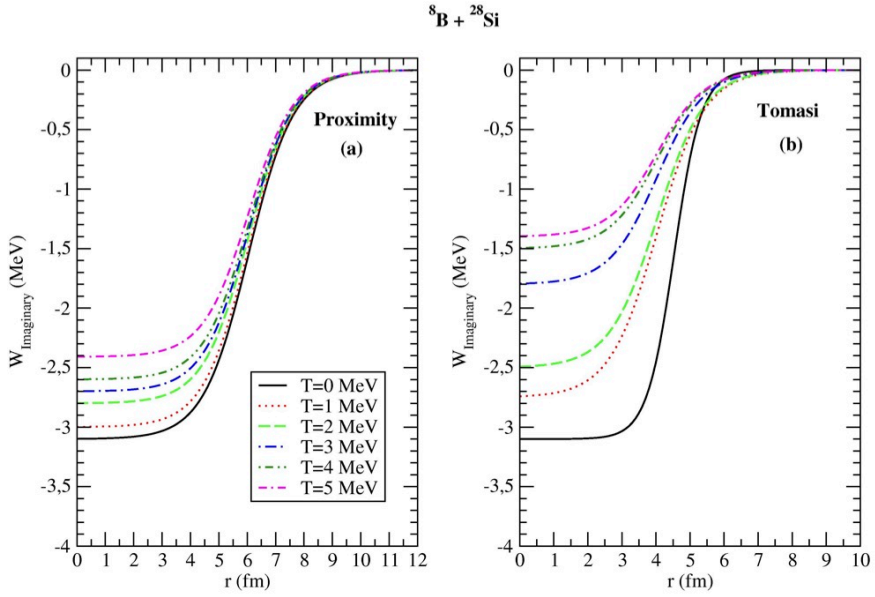

Figure 5. Comparison of the imaginary potentials for different temperature values of ^{8}B + ^{28}Si fusion reaction given in Table 1.

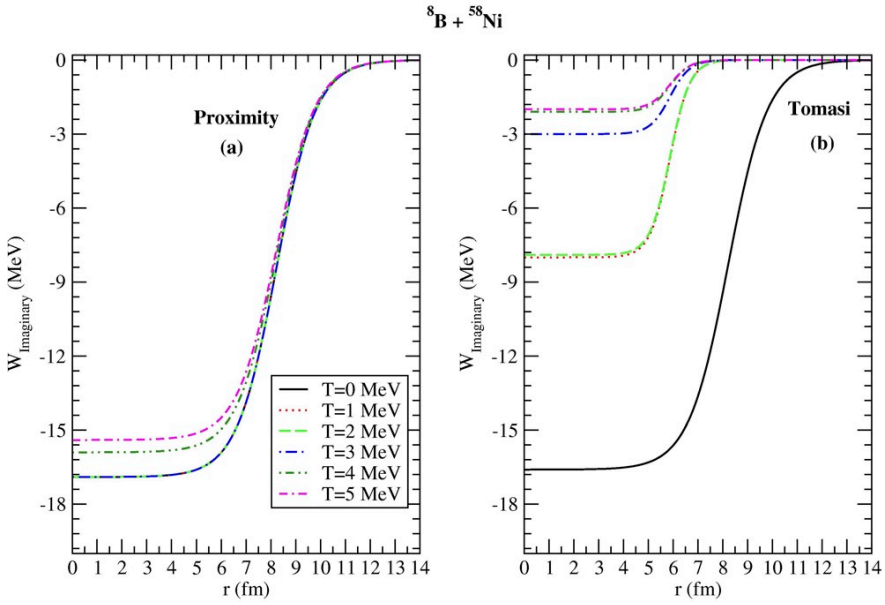

Figure 6. Comparison of the imaginary potentials for different temperature values of ^{8}B + ^{58}Ni fusion reaction given in Table 2.

4. Conclusion

Possible effects of the temperature on the fusion cross-sections and nuclear potentials for the ^{8}B proton halo nucleus with ^{28}Si and ^{58}Ni target nuclei have been investigated as temperature-independent (at T = 0 MeV)

and temperature-dependent (at T = 1, 2, 3, 4, and 5 MeV) by using proximity and Tomasi potentials. It has been seen that the real parts of the nuclear potentials of ^{8}B $+^{28}$Si and ^{8}B $+^{58}$Ni reactions have decreased with increasing temperature. In addition to this, they extend at larger distances and their locations are shifted at smaller distances. Moreover, it has been observed that the effect of temperature on fusion cross-sections is significant. In this respect, it has been noticed that the agreement between fusion cross-sections and experimental data has varied with the temperature. This situation is especially evident in the results with Tomasi potential of ^{8}B $+^{28}$Si and ^{8}B + ^{58}Ni reactions. Therefore, I can say that the fusion cross-sections with Tomasi potential are more sensitive to temperature than proximity potential.

Also, I have determined the values of the potential parameters for all reactions and temperature values. I can conclude that the differences in the values of the parameters given in Table 1 and Table 2 may be a result of proton halo effect. From this point of view, it can be said that it is necessary to obtain new fusion experimental data of the ^{8}B proton halo nucleus with different target nuclei for a better understanding of the fusion interactions of the ^{8}B nucleus.

Consequently, I can say that it will be valuable to apply this approach to other fusion reactions of the ^{8}B proton halo nucleus as temperature-independent and temperature-dependent.

References

[1] Rashdan M, Faessler A, Ismail M, Ohtsuka N. The temperature dependence of the Hi optical potential. Nuclear Physics A 1987; 468: 168-176. doi: 10.1016/0375-9474(87)90322-8

[2] Guo-Qiang L, Gong-Ou X. Optical potential and the fusion barrier of two hot nuclei. Physical Review C 1990; 41: 169. doi: 10.1103/PhysRevC.41.169

[3] Amador-Valenzuela P, Aguilera EF, Martinez-Quiroz E, Lizcano D, Belyaeva TL et al. Mapping σ_p into σ_{fus} for the ^{8}B + ^{58}Ni system. Journal of Physics: Conference Series 2014; 492: 012003. doi: 10.1088/1742-6596/492/1/012003

[4] Pakou A, Stiliaris E, Pierroutsakou D, Alamanos N, Boiano A et al. Fusion cross sections of ^{8}B+ ^{28}Si at near-barrier energies. Physical Review C 2013; 87: 014619. doi: 10.1103/PhysRevC.87.014619

[5] Aguilera EF, Amador-Valenzuela P, Martinez-Quiroz E, Fernández-Arnáiz J, Kolata JJ et al. Above-barrier fusion enhancement of proton-halo systems. Physical Review C 2016; 93: 034613. doi: 10.1103/PhysRevC.93.034613

[6] Aguilera EF, Amador-Valenzuela P, Martinez-Quiroz E, Lizcano D, Rosales P et al. Near-barrier fusion of the ^{8}B $+^{58}$Ni proton-halo system. Physical Review Letters 2011; 107: 092701. doi: 10.1103/PhysRevLett.107.092701

[7] Gómez-Camacho A, Aguilera EF, Lubian J, Gomes PRS. Simultaneous χ^2-analysis of near-barrier fusion and elastic scattering for the proton-halo system ^{8}B $+^{58}$Ni using dynamical Woods–Saxon polarization potentials. Journal of Physics G: Nuclear and Particle Physics 2013; 40: 035103. doi: 10.1088/0954-3899/40/3/035103

[8] Tomasi E, Chen XS, Leray S, Ngô C, Barranco M et al. Calculation of interaction potentials between two heavy ions at finite temperature. Nuclear Physics A 1982; 389: 69-79. doi: 10.1016/0375-9474(82)90291-3

[9] Bansal M, Chopra S, Gupta RK, Kumar R, Sharma MK. Dynamical cluster-decay model using various formulations of a proximity potential for compact non-coplanar nuclei: Application to the ^{64}Ni $+^{100}$Mo reaction. Physical Review C 2012; 86: 034604. doi: 10.1103/PhysRevC.86.034604

[10] Salehi M, Ghodsi ON. The influence of the dependence of surface energy coefficient to temperature in the proximity model. Chinese Physics Letters 2013; 30: 042502. doi: 10.1088/0256-307X/30/4/042502

[11] Sauer G, Chandra H, Mosel U. Thermal properties of nuclei. Nuclear Physics A 1976; 264: 221-243. doi: 10.1016/0375-9474(76)90429-2

[12] Shlomo S, Natowitz JB. Temperature and mass dependence of level density parameter. Physical Review C 1991; 44: 2878. doi: 10.1103/PhysRevC.44.2878

[13] Gharaei R, Zanganeh V. Temperature-dependent potential in cluster-decay process. Nuclear Physics A 2016; 952: 28-40. doi: 10.1016/j.nuclphysa.2016.04.001

[14] Satchler GR. Direct Nuclear Reactions. Oxford, UK: Oxford University Press, 1983.

[15] Thompson IJ. Coupled reaction channels calculations in nuclear physics. Computer Physics Reports 1988; 7: 167-212. doi: 10.1016/0167-7977(88)90005-6

[16] http://www.fresco.org.uk/.

[17] Ngo C, Tamain B, Galin J, Beiner M, Lombard RJ. Calculation of interaction barriers using the energy density formalism. Nuclear Physics A 1975; 240: 353-364. doi: 10.1016/0375-9474(75)90335-8

[18] Ngo C, Beiner M, Tamain B, Lombard RJ, Mas D et al. Properties of heavy ion interaction potentials calculated in the energy density formalism. Nuclear Physics A 1975; 252: 237-252. doi: 10.1016/0375-9474(75)90614-4

[19] Blocki J, Randrup J, Świątecki WJ, Tsang CF. Proximity forces. Annals of Physics 1977; 105: 427-462. doi: 10.1016/0003-4916(77)90249-4

[20] Zanganeh V, Gharaei R, Izadpanah AM. Comparative study for different nuclear proximity potentials applied to quasi-elastic scattering and fusion reactions. Nuclear Physics A 2019; 992: 121637. doi: 10.1016/j.nuclphysa.2019.121637

[21] Gharaei R, Zanganeh V, Wang N. Systematic study of proximity potentials for heavy-ion fusion cross sections. Nuclear Physics A 2018; 979: 237-250. doi: 10.1016/j.nuclphysa.2018.09.032

[22] Dutt I, Puri RK. Systematic study of the fusion barriers using different proximity-type potentials for N = Z colliding nuclei: new extensions. Physical Review C 2010; 81: 044615. doi: 10.1103/PhysRevC.81.044615

[23] Aygun M, Aygun Z. A comprehensive analysis of ^{9}Li $+^{70}$Zn fusion cross section by using proximity potentials, temperature dependent density distributions and nuclear potentials. Revista Mexicana de Física 2019; 65: 573-582. doi: 10.31349/RevMexFis.65.573

[24] Aygun M. Effects of proximity potentials on the cross-sections of ^{6,8}He $+^{65}$Cu halo fusion reactions. Ukrainian Journal of Physics 2019; 64: 5. doi: 10.15407/ujpe64.5.363

[25] Myers WD, Swiatecki WJ. Nuclear masses and deformations. Nuclear Physics 1966; 81: 1-60. doi: 10.1016/0029-5582(66)90639-0